Multiscale controls on thermal spring emergence in France: From national statistics to local scale modelling (Chaudes-Aigues hydrothermal system)

Emmy Penhoët, Laurent Guillou-Frottier, Yannick Branquet, Laurent Arbaret, Bernard Sanjuan, Angélie Portal

Journal of Hydrology: Regional Studies 65 (2026) 103415

Contents lists available at ScienceDirect

Journal of Hydrology: Regional Studies

journal homepage: www.elsevier.com/locate/ejrh

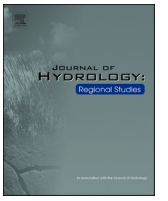

Multiscale controls on thermal spring emergence in France: From national statistics to local scale modelling (Chaudes-Aigues hydrothermal system)

Emmy Penhoët [a,b], Laurent Guillou-Frottier [a,b,*], Yannick Branquet [c], Laurent Arbaret [b], Bernard Sanjuan [a], Angélie Portal [a]

[a] BRGM- French Geological Survey, Orléans F-45060, France
[b] ISTO, UMR 7327, Université d'Orléans, CNRS, BRGM, Orléans F-45071, France
[c] Géosciences Rennes, UMR 6118, CNRS, Université de Rennes, Rennes, France

ARTICLE INFO

Keywords:
Chaudes-Aigues
thermal springs
spatial analysis
numerical modelling
buoyancy driven flow
fault zone

ABSTRACT

Study region: Metropolitan France and a focus on Chaudes-Aigues (French Massif Central)
Study focus: The occurrence of high-temperature thermal springs in amagmatic context raises a fundamental question: why does a hot spring emerge at a given location? This study tries to fix this issue through a multi-scale approach combining statistical and physical analyses. First, a large-scale statistical investigation is conducted at the scale of metropolitan France, based on a database of more than 360 thermal springs. Different parameters are examined to identify a dominant controlling factor governing the spatial distribution and temperature of thermal springs.
A second approach based on thermo-hydraulic modelling is developed and applied to the hydrothermal system of Chaudes-Aigues, hosting the hottest spring in Europe.
New hydrological insights for the region: This statistical approach suggests that hot spring formation results from the complex interaction of these factors. Several model configurations are tested integrating topography and a deep reservoir reaching 190°C identified by geochemical studies. Only models including both elements successfully reproduce all field and geochemical criteria. Models also constrain the infiltration area along a major fault system and indicate long residence times (50 – 200 kyr). These results highlight the key role of coupled structural control, topography and deep fluid circulation in the genesis of thermal springs. Together, this two-step study provides new insights of the thermal spring origin in amagmatic context.

1. Introduction

The emergence of thermal springs (defined as discharges of geothermal waters whose temperature exceeds the averaged ground surface temperature) on the Earth's surface corresponds to a local expression of an underlying hydrothermal system, kilometres in size

Abbreviations: BRGM, Bureau de Recherches Géologiques et Minières; ISTO, Institut des Sciences de la Terre d'Orléans; LGU, Lower Gneiss Unit; UGU, Upper Gneiss Unit; MGC, Margeride Granite Complex.

* Corresponding author at: BRGM, French Geological SurveY, Orléans F-45060, France.
E-mail addresses: e.penhoet@brgm.fr (E. Penhoët), l.guillou-frottier@brgm.fr (L. Guillou-Frottier), yannick.branquet@univ-rennes.fr (Y. Branquet), laurent.arbaret@univ-orleans.fr (L. Arbaret), b.sanjuan@brgm.fr (B. Sanjuan), a.portal@brgm.fr (A. Portal).

https://doi.org/10.1016/j.ejrh.2026.103415
Received 6 February 2026; Received in revised form 31 March 2026; Accepted 1 April 2026
Available online 4 April 2026

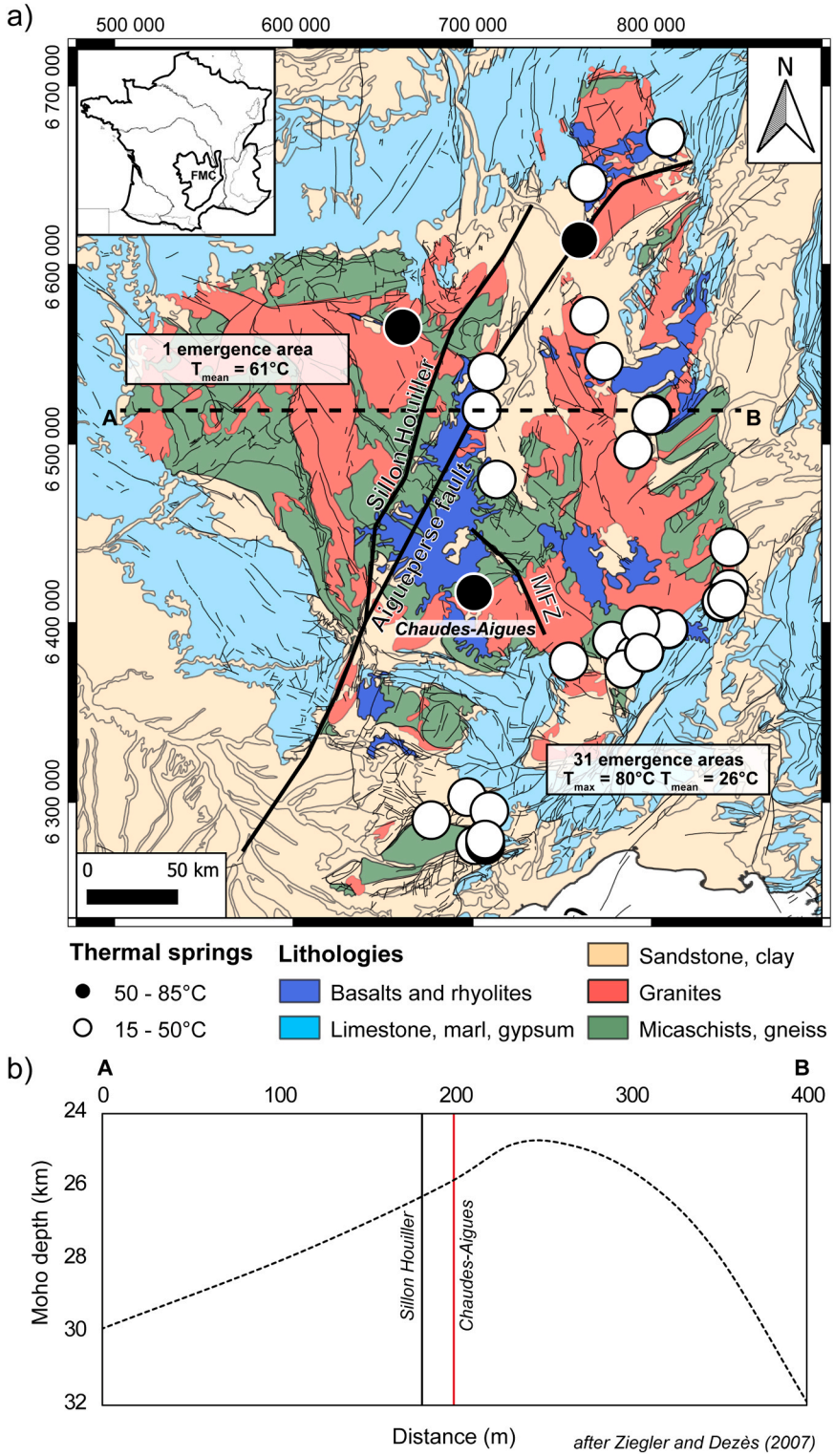

Fig. 1. (a) Thermal springs distribution in the French Massif Central on a simplified geological map (BRGM). (b) Depth of the Moho represented as the thickness of the crust along the AB profile (after Ziegler and Dèzes, 2007). The dashed red line indicates a perpendicular projection of Chaudes-Aigues area on AB profile. One dot may correspond to several springs (around 30 springs at Chaudes-Aigues).

and with a lifespan that can reach tens to hundreds of thousands of years (Andrews et al., 1982; Vasseur et al., 1997; Grasby and Hutcheon, 2001; Allen et al., 2006;; Stober et al., 2016; Foued et al., 2017; Taillefer et al., 2018; Taillefer et al., 2024). In many countries, these surface manifestations of a potential heat resource helped geothermal exploration and led to the development of geothermal power plants (e.g. Larderello in Italy, or The Geysers in California). However, the factors controlling thermal spring emergences remain poorly constrained. For instance, statistical studies have been undertaken on an extensive dataset of more than 6000 geothermal springs (Waring and Blankenship, 1965). Tamburello et al. (2022) analysed the entire dataset with a Random Forest algorithm to improve our understanding on the controlling factors leading to the presence of thermal springs. Among them, terrestrial heat flow, topography, volcanism and extensional tectonics appear to play the most significant role on the occurrence of thermal springs. Yet, depending on the studied criteria, the dominant process may differ. For example, the number of geothermal springs areas seems to be controlled by anomalous terrestrial heat flow, whereas the number of geothermal springs in each area would be controlled by topography. Therefore, it appears that factors controlling the emergence of thermal springs are scale dependent.

In the past, numerous studies were dedicated to the classification of thermal springs (see Zhou et al., 2023 for a review) but rarely to their driving mechanisms. Several hydrogeological processes such as topography-driven or buoyancy-driven flows have been invoked to explain the emergence of thermal springs (Lopez and Smith, 1995; Magri et al., 2016; Taillefer et al., 2018). In addition, local geological and petrophysical factors (such as rock permeability or fault zone architecture) are recognized to play a major role on the efficiency of upward hot fluid circulation (Faulds et al., 2010; Duwiquet et al., 2019; Zhou et al., 2023).

For the specific case of the Pyrenees (south-west France), topographic gradient appears to control the location and temperature of thermal springs (up to 72°C) along the Têt fault (Taillefer et al., 2018). Yet, regional terrestrial heat flow in the Pyrenees is not anomalous, and thermal convection (or buoyancy-driven flow) within the Têt fault would not be sufficiently active to explain emergence of thermal springs, which thus appears as a result of topography-driven flow. In the French Massif Central (central France), the hottest thermal spring in continental Europe (the « Par » spring in Chaudes-Aigues city, 82°C) is located in an area with smooth topography (a few hundreds of meters), and thermal convection is probably much more active to explain the emergence of around 30 thermal springs (Vasseur et al., 1997; Penhoët et al., 2025b). Therefore, at the geothermal field scale, interaction between physical controls of emergence is complex, not unique and deserve further investigations.

Since controlling factors for emergence of thermal springs seem to differ from one case to the other, we begin this study with a large-scale statistical approach (at the scale of metropolitan France) by gathering several datasets: an exhaustive compilation of thermal springs in France is analysed in terms of lithology, topography, heat flow and fault density. This study aims to identify the key factors controlling thermal spring emergence and their interactions. In the second part of our study, we focus on a single geothermal system where numerous field data are available (the emblematic Chaudes-Aigues hydrothermal system). Here we use a physical approach with a 3D numerical thermo-hydraulic model, to understand which process could explain the emergence of thermal springs. In this second approach, numerous field data have been used (terrestrial heat flow, spring location, spring temperature, spring composition and flow rates), and the main objective consists in varying unknown parameters (such as rock permeability) to reproduce field data.

1.1. Regional and local settings

1.1.1. The French Massif Central

1.1.1.1. Geological and geodynamic settings. Variscan history of the Massif Central will not be detailed, although it plays a fundamental role in the current structuring of the region. Indeed, the main fault orientations N030 - 50E and N120 - 150E structuring the study area, typical of regional fracturing, originate from this ancient heritage (Penhoët et al., 2025a). From a hydrothermal point of view, the key factor is the reactivation of these structures over geological time to maintain their high permeability. From a thermal point of view, late Variscan period (~ 280–300 Ma) provides very little information, as the hydrothermal system lifetime ranges from tens to hundreds of thousand years (Iwatsuki et al., 2000; Waber et al., 2017; Dupuy, 2021; Carbajal-Martínez et al., 2024; Wang et al., 2024), which is negligible compared with the time scale of Variscan events.

Tertiary events are fundamental to understand the actual thermal state of our study area (Penhoët et al., 2026). At the end of the Cretaceous and during the Palaeocene, a compressive phase led to a lithospheric bulge in Europe (Ziegler and Dèzes, 2007). During the Eocene, an extensional phase developed across Europe, forming a series of sedimentary basins (European Cenozoic Rift System, Ziegler, 1992). Evidence of this phase can be seen in the central part of the Massif Central (Fig. 1a) such as the Limagne (Michon and Merle, 2005; Dèzes et al., 2004; Merle et al., 2023) or the Malzieu basins (De Goer de Herve, 1991; Penhoët et al., 2025a). The origin of this extensive phase is still discussed (Michon et al., 2003; Michon and Merle, 2005; Dèzes et al., 2004; 2005; Jolivet et al., 2025). Authors agree, however, that a mantle thermal anomaly caused crustal thinning beneath the Massif Central. This anomaly is particularly visible in section AB, Fig. 1b. To the west of the Houiller Sillon, the crust is about 30 km thick. Towards the east it becomes progressively thinner, reaching 25 km beneath the Limagne basin. Crust thickness returns to normal at the eastern edge of the profile (Fig. 1b).

The French Massif Central (FMC) exhibits a large wavelength surface heat flow anomaly (greater than 90 $mW{\cdot}m^{-2}$). At the scale of Western Europe, several surface heat flow maps clearly illustrate this ~800 km long anomalous surface heat flow signature, from the southwest Massif Central to the Upper Rhine graben in Germany (see Fig. 2b in Cloetingh et al., 2010; Fig. 5 in Majorowicz and Wybraniec, 2011, or Fig. 3b in Guillou-Frottier et al., 2024).

Although different geodynamic processes (Alpine subduction-induced, shear-heating, lateral mantle flow) have been suggested to

cause this anomalous mantle heat flow, the main consequence is that the first kilometres of the crust are heated from below by a heat flow reaching 80–90 mW·m^{-2} (i.e. a large mantle heat flow component complemented with the radiogenic component of the crust). This is the basal thermal boundary condition which will be assumed in the following numerical models.

1.1.1.2. Thermal springs distribution. Thermal springs are unequally distributed throughout the Massif Central (Fig. 1a). To the north-west of the Sillon Houiller and the Aigueperse Fault, only one hydrothermal system is known. (Evaux-les-Bains, with a maximum temperature of 61°C). In contrast, in the south-east, on the opposite side of the Sillon Houiller, there are 31 areas where thermal springs emerge. The average temperature of the springs is 26°C. The hottest of these is the Par Spring (82°C), part of the Chaudes-Aigues hydrothermal system. The second part of this study is focused on this hydrothermal system which seems to be located on the most favorable part of the FMC.

1.1.2. Chaudes-Aigues

1.1.2.1. Geological settings. The thirty thermal springs of the Chaudes-Aigues area are located near the northern edge of the Margeride Granitic Complex (MGC, Fig. 2a). The MGC was emplaced into the Variscan basement, made of metamorphic units (Lower Gneiss Unit, LGU and Upper Gneiss Unit, UGU), during the late Carboniferous (~ 310 Ma) (Talbot et al., 2005). Its emplacement is associated with post-orogenic extension and is accompanied by a network of fractures and faults that have been reactivated during subsequent tectonic episodes (Talbot et al., 2005 and Penhoët et al., 2025a for a more detailed geological context). The springs are located at the edges of a major NW-SE fault system crosscut by 2 other Variscan fault zones (Gibert et al., 1975; De Goer de Herve, 1991; Penhoët et al., 2025b), N050E and N150E (Fig. 2b) creating a very high permeability zone. Theses faults would crosscut the MGC beneath the town. Gravity studies have shown that the MGC is dipping to the north and lies at a shallow depth (few hundred meters) beneath the town (Talbot et al., 2005; Penhoët et al., 2026).

1.1.2.2. Hydrogeological setting. The 30 thermal springs of the Chaudes-Aigues area reach temperatures between 50 and 82°C, making the Par spring one of the hottest natural springs in continental Europe. Most references report a total flow rate of approximately 500 l·min^{-1} for the entire Chaudes-Aigues hydrothermal system (Blanquet et al., 1950; Cailleaux et al., 1976; Vasseur et al., 1997), although values as high as 700 l·min^{-1} have also been mentioned (Bérard et al., 2002), with the discharge remaining constant throughout the year. The emergence area, in the gneissic units, is characterized by a high density of brittle structures (Fig. 2b). These NW-SE faults intersect the whole MGC, creating a favourable setting for hydrothermal activity. Further south in the MGC (10 km), located in the same fault zone, another thermal spring, the "La Chaldette" spring emerges at 35°C in the granite laccolith (Fig. 2b).

The Chaudes-Aigues springs represent a mixture of surface water and a contribution from a deep endmember (Vasseur et al., 1997; Penhoët et al., 2025b). The meteoric waters would infiltrate to the south via a N150E fault zone (hosting the La Chaldette spring, Fig. 2). Its geochemical composition corresponds to the surface signature of the mixture of thermal waters. This fault zone would allow meteoric waters to be drained at shallow depths, giving rise to thermal springs such as La Chaldette, but also at depth to supply a deep reservoir, whose temperature has been estimated at 190°C (Penhoët et al., 2025b). This reservoir is thought to lie on the northern edge of the MGC which dips to the north and lies at shallow depth beneath the town, as confirmed by recent gravity measurements (Penhoët et al., 2026). The major Variscan faults N050E, characterised by crushed mylonites, reactivated over geological time, are thought to be the main drains of the system (Penhoët et al., 2026). This fault orientation is intersected by a N150E fault zone, once again resulting in

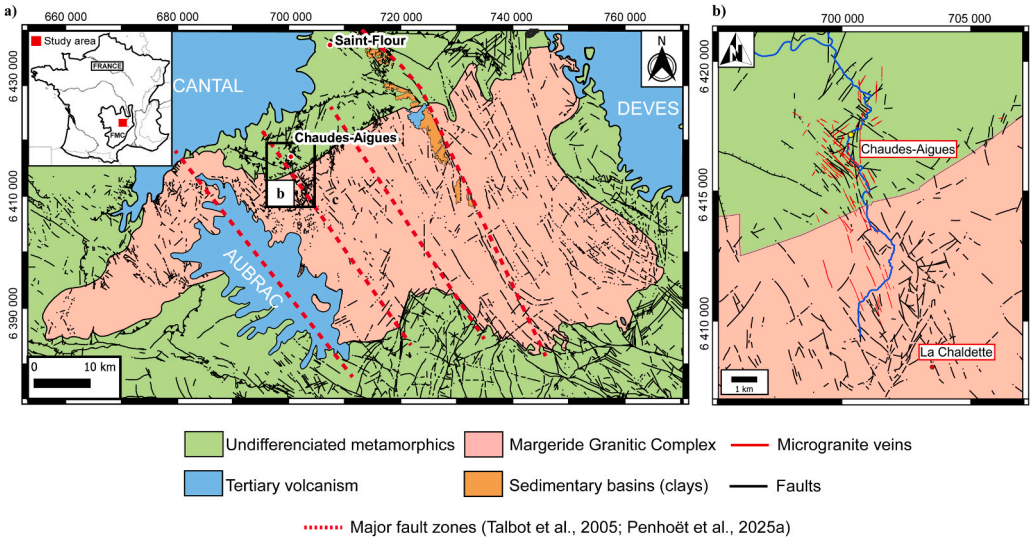

Fig. 2. Geological maps of the (a) MGC cut by the various major fault zones (red dashed lines) and (b) zoom on the Chaudes-Aigues area.

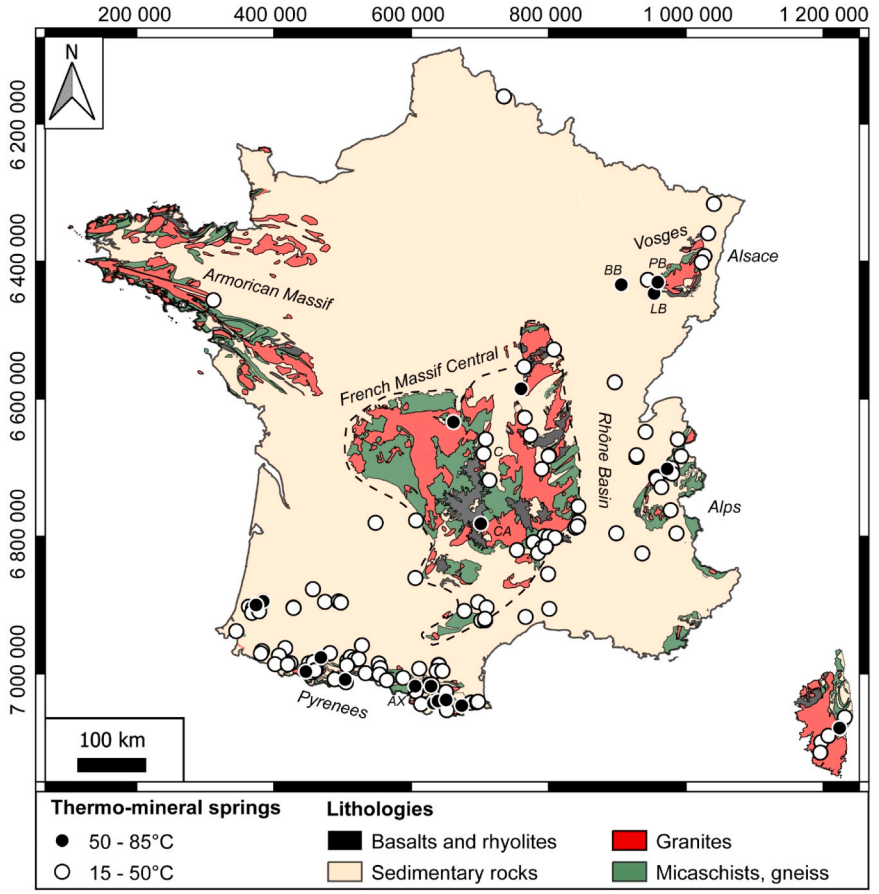

Fig. 3. Distribution of thermal springs (according to the Banque du Sous-Sol, BSSEAU, BRGM) in France. The background map corresponds to the 2 M geological map (BRGM). PB is for Plombières-les-Bains, BB Bourbonne-les-Bains, LB Luxeuil-les-Bains, CA Chaudes-Aigues, AX Ax-les-Thermes and C Chamalières. One dot may correspond to several springs (around 30 springs at Chaudes-Aigues and Plombières-les-Bains).

very high permeability around the thermal springs.

1.2. Methods and strategies

This section describes our two complementary approaches, the statistical one at the scale of metropolitan France, and the physical one at the scale of the Chaudes-Aigues hydrothermal system. The objectives are identical and are driven by the same question: why thermal springs emerge at a specific location and what is the driving mechanism? The first approach, statistical and at the scale of metropolitan France, requires a large number of data. The second approach, physical and focused on a particular hydrothermal system, requires a large number of local field data (geological, geochemical and geophysical) in order to constrain our numerical modelling strategy.

1.2.1. At the scale of metropolitan France

For the following analysis, a spring is said to be thermal if its temperature exceeds the annual average of the ground surface temperature. In France, the average annual ground temperature was 14.4°C and 14.5°C in 2022 and 2023, respectively (French National Temperature Indicator, Infoclimat, www.infoclimat.fr), so any spring with a temperature above 15°C is considered as thermal. Using this definition, more than 368 springs have been identified in France (BSSEAU BRGM, https://infoterre.brgm.fr/page/eaux-souterraines-bsseau, Annales des mines, 1998, https://www.annales.org/ri/1998/ri05-98/inventaire.pdf). In this database, each data represents one single thermal spring with single measurements (e.g. spring temperature is not an average annual value). However, the total number of springs in an area may differ from the real number of springs. As an example, in this database, only two sources over the 30 thermal springs at Chaudes-Aigues are reported. The springs have been divided into two categories: between 15 and 50°C thermal springs and between 50 and 85°C very hot thermal springs. The previous global database (Waring and Blankenship, 1965 and Tamburello et al., 2022) contained only 152 thermal springs in France.

1.2.1.1. Topography analysis. Identified as a key parameter in fluid circulation, topography controls both fluid infiltration but also the

distribution of thermal springs at the surface (Taillefer et al., 2018). To identify the influence of topography, a Digital Elevation Model (DEM) was used. The DEM data are provided in raster grid format with a 25 m pixel spatial resolution and a maximum vertical accuracy of 2.5 m (IGN, 2011). For each spring from the database, within a 10 km radius, the difference between the maximum elevation and the spring elevation was extracted from the DEM. This method provides a first-order approximation of the topographic gradient surrounding each spring.

1.2.1.2. Fault density analysis. The fault density analysis uses the same workflow as in Penhoët et al. (2025a), adapted here to a different assemblage of geological maps. Faults were extracted from thirteen 1:50,000 geological maps and analysed using a 500 m × 500 m grid, with cumulative fault lengths per cell classified using the Jenks natural breaks method (Jenks algorithm implemented in QGIS; Jenks, 1967). Within a radius of 10 km, the average value of cumulative fault length has been calculated.

1.2.2. At the scale of Chaudes-Aigues

As demonstrated in previous studies, the establishment of convective regimes (buoyancy-driven flow) in a fault zone depends directly on petrophysical properties and fault zone thickness and width (Malkovsky and Magri, 2016; Duwiquet et al., 2021; Penhoët et al., 2025a). Topography-driven flow may also lead to advective regimes (Lopez and Smith, 1995; Taillefer et al., 2018). Here, a parametric study was carried out to determine the controlling factors and mechanisms leading to the establishment of the Chaudes-Aigues hydrothermal system. Using Comsol Multiphysics™ software, models with or without topography, and with or without a deep reservoir have been tested.

As in Guillou-Frottier et al. (2013) where Comsol Multiphysics™ software (Finite Element Modelling) was used, Darcy law is coupled with heat transfer equation and mass conservation respectively:

$$\vec{v} = - \frac{k}{\mu_f}\left(\nabla \vec{P} - \rho_f \vec{g}\right)\# \tag{1}$$

$$\rho_s Cp_s \frac{\partial T}{\partial t} = \nabla(\lambda \bullet \vec{\nabla} T) - \rho_f C_f \vec{v} \bullet \vec{\nabla} T + A\# \tag{2}$$

$$\frac{\partial \varnothing \rho_f}{\partial t} + \nabla.(\rho_f . \vec{v}\ ) = 0\# \tag{3}$$

where v is the Darcy velocity ($m{\cdot}s^{-1}$), k (m^2) the permeability of the flow medium, μ_f (Pa·s) the dynamic viscosity of the fluid, ρ_f ($kg{\cdot}m^{-3}$) the density of the fluid, g the acceleration of gravity (by convention, 9.81 $m^2{\cdot}s^{-1}$), T (°C) temperature, t (s) time, ρ_s ($kg{\cdot}m^{-3}$) the rock density, Cp_s ($J{\cdot}kg^{-1}{\cdot}K^{-1}$) the specific heat of rocks, λ ($W{\cdot}m^{-1}{\cdot}K^{-1}$) the equivalent thermal conductivity of the porous media (power law), ρ_f the fluid density, C_f the fluid specific heat ($J{\cdot}kg^{-1}{\cdot}K^{-1}$), A ($W{\cdot}m^{-3}$) the heat production and ϕ the porosity. Fluid is considered as pure water.

For each model configuration (with or without topography and with or without reservoir), two different simulations were computed. First, a simulation corresponds to a conductive regime where fault zones are not activated (very low permeability). This conductive regime is then used as the initial conditions for the second simulation. This second simulation is performed with the physical properties (permeability) of the fault zones.

Physical properties such as thermal conductivity, heat capacity, porosity, rock density (see Table 1) were estimated thanks to field observations and literature data (Brace, 1984; Lucazeau et al., 1984; Sonney and Vuataz, 2009; Moeck, 2014, Neuzil, 2019).

The dynamic viscosity of the fluid is temperature-dependent (e.g. Rabinowicz et al., 1998):

$$\mu(T) = 2.414.10^{-5}.\exp^{\frac{570}{(T+133)}}\# \tag{4}$$

and the density of water depends on both pressure and temperature (see state equation in Launay, 2018; Appendix A in Guillou-Frottier et al., 2020, Penhoët et al., 2025a)

The main unknown remains the permeability value for each formation. The MGC and the metamorphic units are considered, in the absence of fracturing, as impermeable. The increase in pressure at depth tends to seal the fractures and thus causes a decrease in the permeability of the units:

Table 1
Physical parameters used for rocks and fluid in 3D modelling. These values have been obtained from different studies (Smith and Chapman 1983, Rabinowicz et al. 1998, McKenna and Blackwell, 2004, Guillou-Frottier et al. 2013, Taillefer et al. 2018, Duwiquet et al. 2019). Φ stands for porosity, k_0 highest permeability reach by the unit (m^2), λ_s solid thermal conductivity ($W{\cdot}m^{-1}{\cdot}K^{-1}$), ρ density ($kg{\cdot}m^{-3}$), Cp_s Solid heat capacity ($J.kg^{-1}.K^{-1}$), λ_f fluid thermal conductivity ($W{\cdot}m^{-1}{\cdot}K^{-1}$), Cp_f fluid heat capacity ($J{\cdot}kg^{-1}{\cdot}K^{-1}$) and A heat production ($W{\cdot}m^{-3}$).

	Φ	k_0	λ_s	ρ	Cp_s	λ_f	Cp_f	A
Metam. units	0.05	10^{-18}	2.9	2700	1000	0.6	4200	0
MGC	0.05	10^{-18}	2.7	2700	1000	0.6	4200	3×10^{-6}
Fault zones	0.1	$10^{-15} - 5 \times 10^{-14}$	3.1	2700	1000	0.6	4200	0

$$k_u(z) = k_{0_u}.\exp^{\frac{-z}{\delta}} \# \quad (5)$$

where $k_u(z)$ is the permeability of each unit u (m^2), k_{0_u} is the highest permeability (Table 1) reached by the unit (at the surface) and z is the depth (m) (Garibaldi et al., 2010). The length δ (m) characterizes the intensity of the decrease in permeability with depth. A δ value of 1500 m has been chosen, in accordance with published permeability variations with depth (Ingebritsen and Manning, 2010; Saar and Manga, 2004).

1.2.2.1. Meshing and geometry. The models have all an identical geometry, based on the geological maps covering the MGC (n°812 Vic-sur-Cere, 813 Chaudes-Aigues, 814 Saugues, 815 Cayres, 836 Entraygues-sur-Truyère, 837 Nasbinals, 838 Saint-Chély-D'Apcher, 839 Langogne, 859 Decazeville, 860 Espalion, 861 Saint-Geniez-D'Olt, 862 Mende, 863 Le Bleymard) and by the emplacement model of the MGC proposed by Talbot et al. (2005). Geometric simplifications have been made, particularly at the extremities of the MGC, which are represented here as vertical due to the lack of data on its deep geometry. The major fault zones (see Fig. 2a and Fig. 4a) cross-cutting the MGC have been represented according to the geological maps (thickness, location) and Talbot et al. (2005) emplacement model: Aubrac, Chaudes-Aigues, Loubaresse, Margeride, and East fault zones (noted FZ 1, FZ 2, FZ 3, FZ 4, and FZ 5 in Fig. 4). Models therefore present 3 main domains: the MGC, fault zones and the host rock made up of metamorphic units (Fig. 4a).

The waters of the Chaudes-Aigues thermal springs are believed to come from a deep and hot reservoir located in the MGC reaching 190°C (Penhoët et al., 2025b). This is represented by a fourth domain on the northern edge of the MGC. Its influence is tested below. Its lateral extension (SW-NE) was determined by the chemical composition of the springs present at the northern edge of the MGC from Penhoët et al. (2025b) (red dots, Fig. 4b). Geochemical studies have shown that these springs originated from a mixture of the same deep reservoir and surface water (Penhoët et al., 2025b). The reservoir has the same physical properties than the MGC, except in the intersection with FZ2 (Fig. 4) where its permeability is the same than the fault zone. The dimensions of these geometries are summarised in Table 2:

The upper surface of the model corresponds to the current topography of the study area. This 25 m resolution Digital Elevation Model comes from the Institut Géographique National (BD-Alti©, https://geoservices.ign.fr/bdalti). The highest altitude corresponds to the Cantal (1615 m a.s.l) and the lowest is in the south-west corner of the model (255 m a.s.l). In order to ensure a consistent decrease in permeability with depth across the entire model (Eq. 1), the geometry was vertically shifted by −1615 m, so that the maximum DEM elevation coincides with the z = 0 reference of the model.

The mesh consists of more than 300,000 tetrahedra. The size of mesh elements is based on the permeability value. In areas of low permeability (host rocks), meshing is coarse (minimum size of 100 m) but extremely fine in the fault zone (high permeability) (maximum size of 20 m).

1.2.2.2. Boundary conditions

1.2.2.2.1. Thermal conditions. At the upper surface of the model, a temperature of 10 °C was fixed except for the Chaudes-Aigues fault zone, which hosts the Chaudes-Aigues and La Chaldette springs (FZ 2, Fig. 5a). To reproduce temperature variations such as those due to thermal springs, a mixed thermal boundary condition has been applied. This was previously used by Magri et al. (2016) or Taillefer et al. (2018):

$$Q = h(T_0 - T) \quad (7)$$

where Q is the surface heat flow ($W{\cdot}m^{-2}$), h a heat transfer coefficient ($W{\cdot}m^{-2}{\cdot}K^{-1}$) and T_0 the fixed surface temperature (10°C). The value of h was selected on the basis of a parametric study to reproduce, in a conductive regime (i) a surface temperature close to 10°C, (ii) a surface heat flow close to 100 $mW{\cdot}m^{-2}$. Its value has to be between 0.01 and 0.07 $W{\cdot}m^{-2}{\cdot}K^{-1}$. For the parametric study its value is fixed at 0.04 $W{\cdot}m^{-2}{\cdot}K^{-1}$. According to regional data, a constant heat flow of 85 $mW{\cdot}m^{-2}$ is imposed at the base of the model (Lucazeau and Vasseur 1989). The lateral borders were thermally insulated (metamorphic units). At the northern edge of the model,

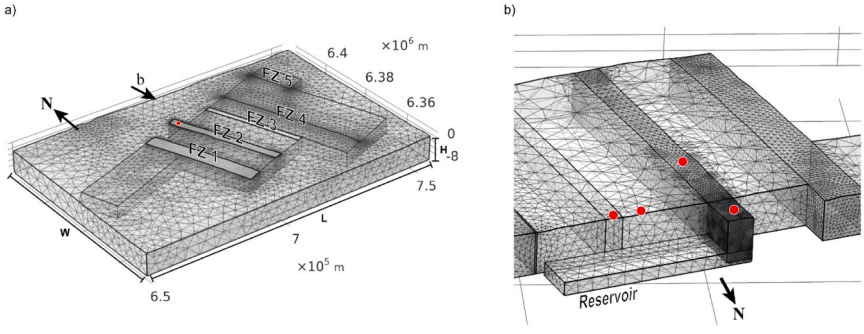

Fig. 4. (a) Overall geometry of the model with the main fault zonescutting the MGC. These are included in the metamorphic units (big rectangular domain). (b) northern view of the Chaudes-Aigues fault zone crossing the assumed reservoir at depth. The red dots correspond to the thermal springs sampled by Penhoët et al. (2025b), which have been used to determine the location of the deep reservoir (see Section 2.2.2).

Table 2
Dimensions of the different domains. Height measurements are taken from the surface of the model, except for the deep reservoir located between 4.5 and 6 km at depth.

	Width (km)	Height (km)	Length (km)
Host rock	106	8	70
MGC	91	5	50
FZ 1	5	5	38
FZ 2	3	5	39
FZ 3	2	5	34
FZ 4	0.2	5	50
FZ 5	0.1	5	15
Reservoir	22	1.5	5

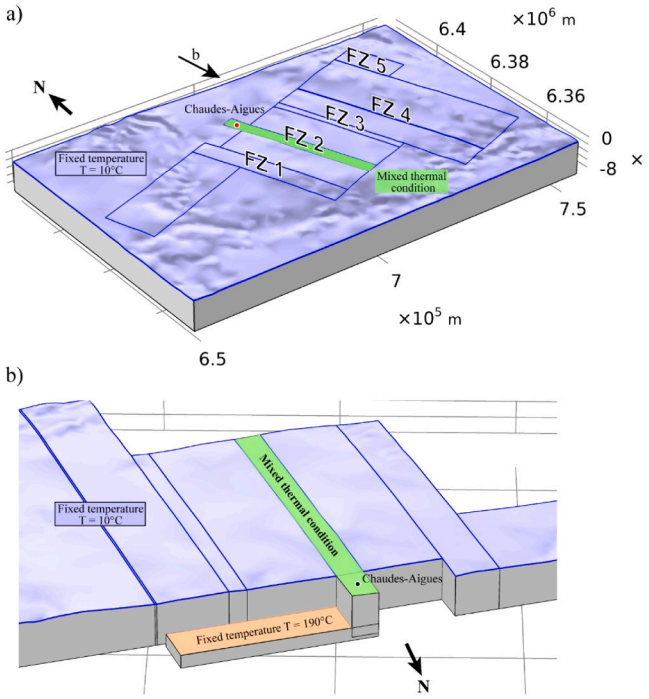

Fig. 5. (a) Thermal boundary conditions used for all models (with or without topography), (b) zoom on the northern edge of the granite with a reservoir represented as a surface with an imposed temperature of 190°C. In the case of models without reservoir this condition disappears.

the deep reservoir is characterised by imposing at its surface (at a depth of 4.5 km) a fixed temperature of 190°C (Vasseur et al., 1997; Penhoët et al., 2025b) (Fig. 5b).

1.2.2.2.2. Flow conditions. The surface pressure is equivalent to the atmospheric pressure (10^5 Pa). A no flow condition was imposed on lateral sides and bottom of the model (metamorphic units). All internal boundaries are considered as continuous.

1.2.2.3. Criteria to be reproduced. To obtain results that are as robust as possible, a series of criteria and parameters will have to be reproduced by the 3D numerical models. Firstly, a geographical criterion: Chaudes-Aigues and La Chaldette springs will have to be spatially reproduced at locations close to reality. They are about 10 km apart in the metamorphic units and the MGC respectively (Fig. 2b). Their temperatures are also key criteria for validating the results. Concerning the Chaudes-Aigues area, which includes around 30 thermal springs, the objective is to reproduce the temperature of the Par Spring (the hottest, measured at 80–82°C). For the La Chaldette spring, the 35°C of the borehole (formerly a natural spring) will have to be reproduced. Then, from a flow rate point of view, the global discharge of the 30 Chaudes-Aigues springs will have to be reproduced. To ensure that the commonly reported total flow rate of 500 l·min^{-1}, the upper estimate value of around 700 l·min^{-1} will be used. This flow will be decomposed into "deep" and "surface" components. The thermal waters of Chaudes-Aigues have been identified as a mixture of 65% meteoric water and 35% deep endmember contribution (Vasseur et al., 1997; Penhoët et al., 2025b). These different flow rates are calculated as an integral of the Darcy velocity across a defined surface. These calculations are detailed in Fig. 6. Finally, the impluvium, identified as the MGC and more precisely the N150E fault zone to the south of Chaudes-Aigues (Penhoët et al., 2025b) should also correspond.

The following numerical results correspond to final state (steady state regime) after 500 kyr of transient evolution.

1.3. Results

1.3.1. Factors influencing thermal spring distribution in France

1.3.1.1. Heat flow. Fig. 7 illustrates the heat flow map of France based on the study by Lucazeau and Vasseur (1989). In France, some regions have an average heat flow, notably the Armorican Massif, the Pyrenees, the South of France and the Alps, with values between 60 and 80 mW·m^{-2}. While these heat flow values are not anomalously high, mountainous regions (Pyrenees, Alps) are very rich in thermal springs. The temperature of most of these springs ranges between 15 and 50°C, but some are above 50°C.

The Massif Central, the Rhône basin and Alsace have much higher heat flow values (90–110 mW·m^{-2}). These areas are characterised by numerous thermal springs, including the hottest in Europe, such as the Par Spring in Chaudes-Aigues. There are also thermal springs at Plombières-les-Bains, Luxeuil-les-Bains and Bourbonne-les-Bains (PB, LB and BB respectively in Fig. 3), where surface heat flow is relatively high, and spring temperatures exceed 50°C. The springs are less abundant than in the previous case, but hotter on average.

The thermal spring-heat flow relationship is not that simple, as already observed in North America (Ferguson and Grasby, 2011). When we compare the heat flow values, represented by the isolines, with the location of the thermal springs, high heat flow value does not lead to a high emergence temperature (Armorican Massif, Rhone basin). By contrast, regions with low heat flow can produce very hot thermal springs, as in the Pyrenees (Fig. 7, T > 50 °C).

Although heat flow is an initial approach to analysing the distribution of thermal springs in France, it is not sufficient. To refine this analysis, other criteria such as fault density, topography and lithology of the hydrothermal system will also be taken into account in the following sections.

1.3.1.2. Host lithology. The database used here indicates the lithology hosting a potential hydrothermal system and a deep reservoir for each spring. Using the 2 M geological map (Fig. 1) and the lithologies cited in the inventory (BSSEAU BRGM, Annales des mines, 1998) four simplified categories have been created: sedimentary rocks (sandstone, clay, sand, limestone, marl and gypsum), granites, metamorphic rocks (micaschists, gneiss, schists) and volcanic rocks (basalts and rhyolites).

The host lithologies in the database (BSSEAU and Annales des mines, 1998) are based on field reports carried out on each spring. When the data is available, it will be used. Conversely, when it is not provided, the spring lithology of the 2 M geological map will be considered. This can lead to uncertainties such as the Chaudes-Aigues springs, which are in metamorphic units but associated with a granitic reservoir (Vasseur et al., 1997; Penhoët et al., 2025b). As the data does not appear in the inventory, these are considered to come from a metamorphic hydrothermal system rather than granitic. Of the 368 springs counted, 2 are hosted within volcanics, 159 within granitic rocks, 56 within metamorphic rocks and 151 within sedimentary rocks (Fig. 8).

The granite-hosted hydrothermal systems have both the largest number of springs and some of the highest temperatures, with a maximum of 77.8°C (« Source Rossignol », Ax-Les-Thermes, AX Fig. 3). The average temperature of these springs is 41°C. Metamorphic rocks also host very hot thermal springs reaching 82°C (« Source du Par », Chaudes-Aigues, CA Fig. 3), with an average value of 37°C.

Sedimentary rocks have many springs, but their temperatures are lower, averaging 30°C, with a maximum of 62°C (« Source no. 10 », Bourbonne-les-Bains, BB Fig. 3). The few springs associated with volcanic rocks are relatively cold (27°C on average), with a maximum temperature of 28°C (« Source Saint-Martin », Chamalières, C Fig. 3).

1.3.1.3. Topography. The results fall into two groups (Fig. 9). The first group covers small elevation changes (less than 1 500 m), with an average temperature of 32°C and a maximum temperature of 80°C (elevation change of 644 m). All four types of lithologies are represented. The second group, with a higher elevation change (between 1 500 and 2 900 m), has a higher average value (39 °C) and a maximum of 77.8 °C. Here, springs in granitic (red dots) and metamorphic rocks (green dots) clearly predominate (Fig. 9b).

It should be noted that the spring temperatures belonging to the sedimentary lithology type are not directly linked to elevation change: temperature varies little as the difference in altitude increases or decreases. Temperatures of springs linked to basement rocks

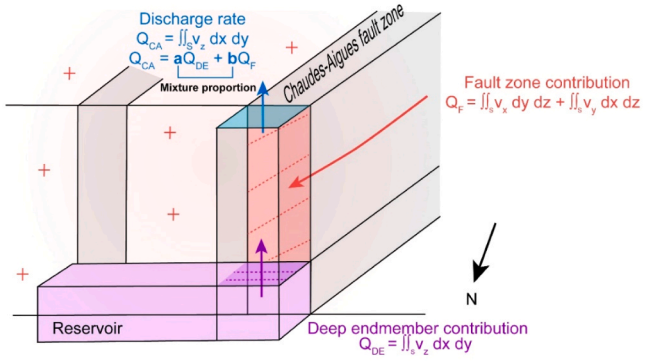

Fig. 6. Calculation of different flow rates and mixing ratios in numerical models.

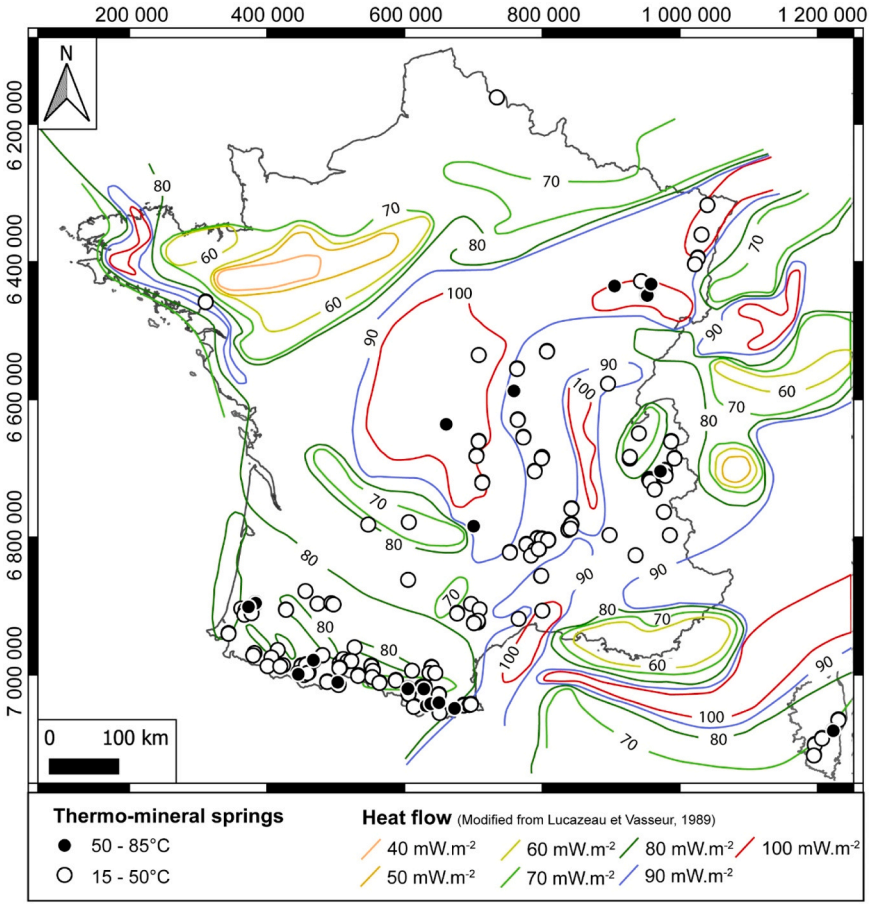

Fig. 7. Distribution of thermal springs as a function of heat flow in France. Heat flow contours are extracted from the heat flow map of Lucazeau and Vasseur (1989).

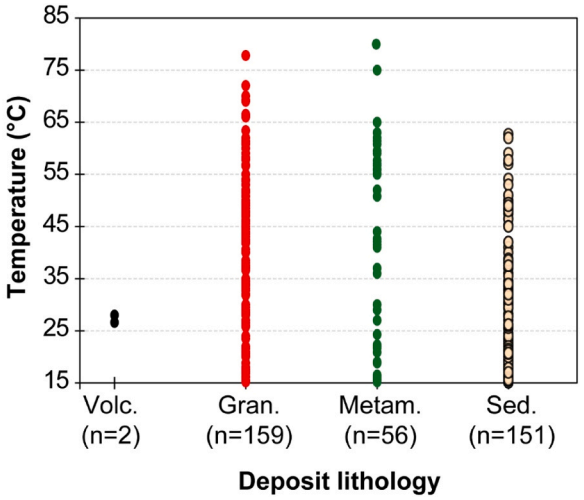

Fig. 8. Temperature of the 368 springs according to the lithology of the hydrothermal system. Volc = Volcanic rocks, Gran = Granites, Metam = Metamorphic rocks, Sed = Sedimentary rocks. Temperature from database correspond to single measurements, not mean annual values.

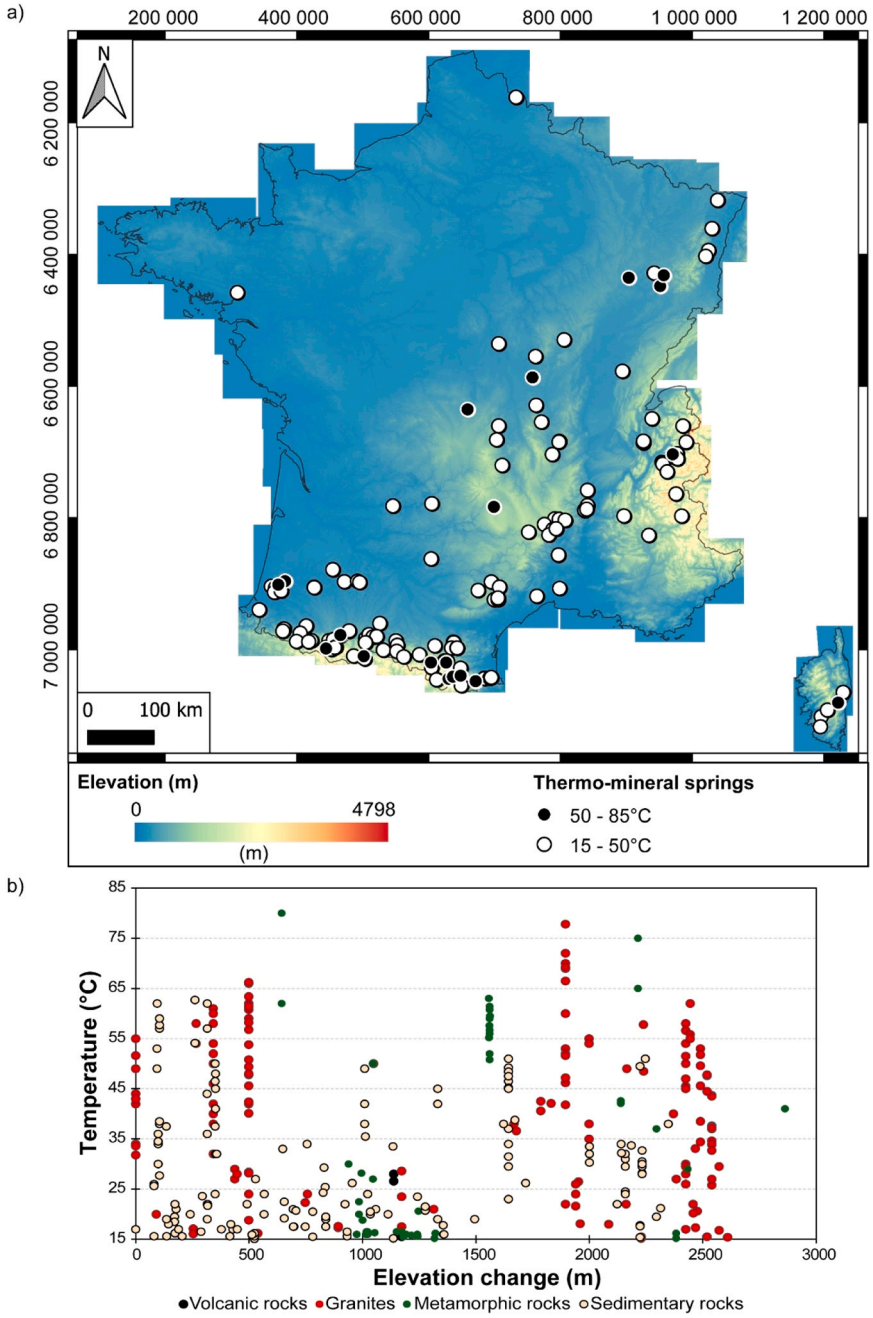

Fig. 9. (a) Map showing the distribution of thermal springs in France as a function of topography. (b) Temperature of springs as a function of maximum difference in elevation within a 10 km radius around each spring.

(granites and metamorphic rocks), in contrast, do not behave in the same way. More springs emerge when the elevation change is high (the second group mentioned above) with higher temperatures. These types of system are therefore more influenced by the surrounding topography.

1.3.1.4. Fault density. The thermal springs are mainly located in densely faulted areas (Fig. 10a). There are a few exceptions, notably in the Aquitaine Basin (south-west of France). Then, results show that an optimum fracturing density permits the highest source temperatures to be reached (Fig. 10b). The highest temperatures (up to 82°C) are found between approximatively 50 km and 100 km of cumulative length, which are not threshold values, but which include the larger number of high temperature springs. For lower densities, the springs are numerous but their maximum temperature decreases, with values not exceeding 65°C. Conversely, for more

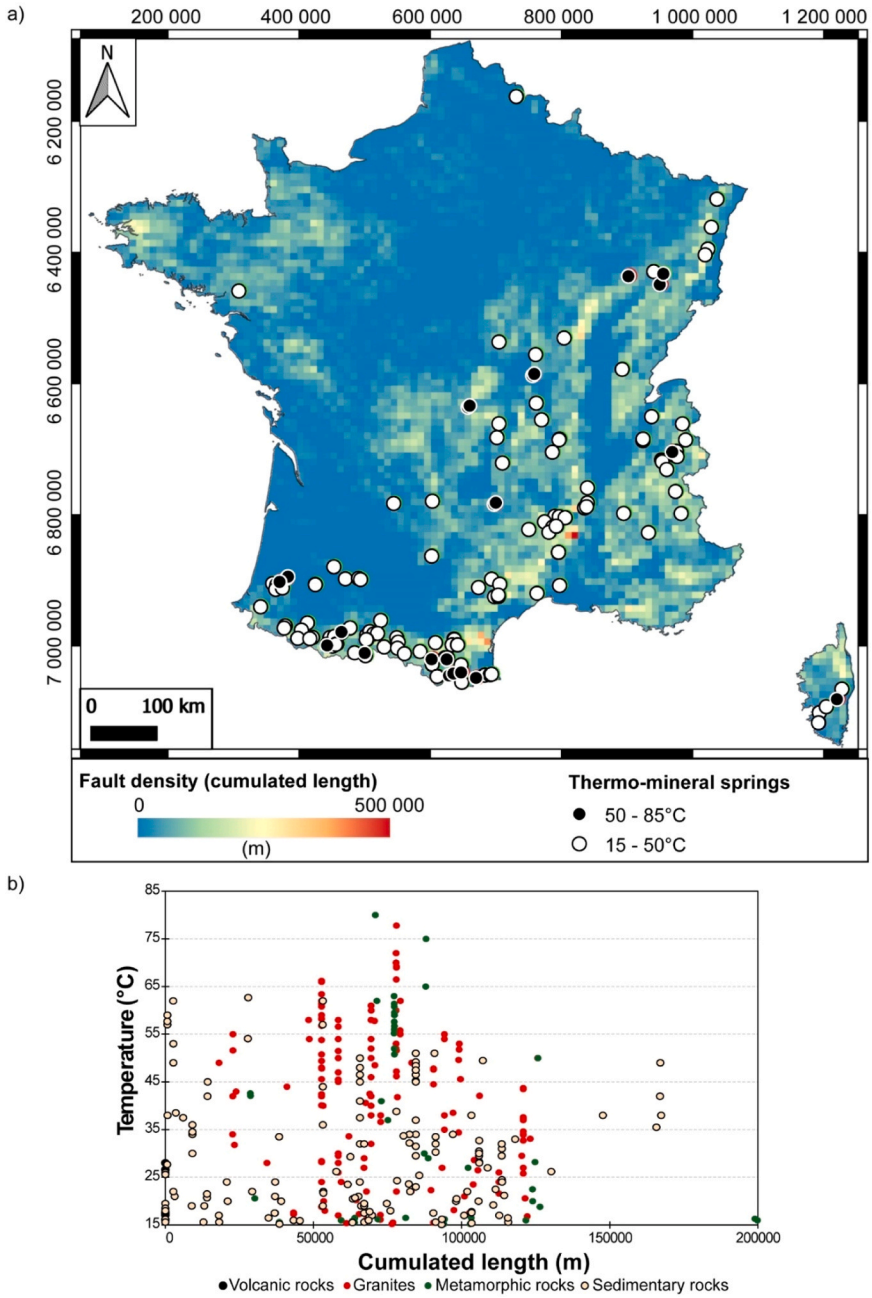

Fig. 10. (a) Map showing the distribution of thermal springs in France as a function of fault density. (b) Temperature of springs as a function of average fault density within a 10 km radius around each spring.

densely faulted areas (> 100 km), there are few springs and temperatures are even lower. These do not exceed 55°C. However, it should be noted that for these density values, the minimum temperatures are high (35°C compared with 15°C for the previous groups). As regards lithologies, it can still be seen that the temperatures of springs in sedimentary environments are not controlled by fracturing at first order; they spread over all fault density values (Fig. 10b). Basement rocks, however, are confined within the window of optimum cumulative length values mentioned above. Outside this optimal range of values, the temperature of the springs falls significantly.

The Chaudes-Aigues hydrothermal system, which is our case study at the hydrothermal system scale, fall within these optimal range of fault density. This specific site will provide an understanding of the interactions between topographic gradient, heat flow and fracturing.

1.3.2. Results for the Chaudes-Aigues hydrothermal system

To determine the control factors of the hydrothermal system, we present our results of numerical modelling following four quantified criteria that have to be reproduced as a function of tested fault permeabilities. The observed values to reach are represented by a dotted red line in Fig. 11. Spatial criteria also must be reproduced, such as the location of thermal springs and the location of the recharge zone.

1.3.2.1. Spring temperatures. The first two criteria correspond to the temperature of the Par and La Chaldette springs along the fault zone FZ2 (Fig. 4b). Concerning the Par Spring (Fig. 11a), its temperature is only reproduced for two configurations involving the presence of the deep reservoir with (blue line) or without (red line) topography. The springs reproduced reach up to 90°C. Without the reservoir (yellow and green lines), the springs do not exceed 60°C, so the Par Spring is not reproduced (Fig. 11a).

The La Chaldette spring is easier to reproduce because of its lower temperature. Three configurations were successful: those with topography and with (blue line) or without (green line) reservoir, and the one without topography or reservoir (yellow line, Fig. 11b). Temperatures range from 35 to 45°C. Nevertheless, without topography and with a reservoir (red line), the La Chaldette spring cannot be reproduced, whatever the permeability of the fault zone (Fig. 11b).

1.3.2.2. Mixing coefficients. The mixing coefficients for Chaudes-Aigues springs vary between 30% and 40% for the deep endmember and 60–70% for surface waters (Penhoët et al., 2025b). The two configurations without deep reservoirs do not reproduce mixing coefficients close to those found in geochemical studies (yellow and green lines, Fig. 11c). Only 10% of the total flow would come from the deep reservoir, which is too low. The configuration without topography but with reservoir (red line) reproduces the mixing coefficients for a small range of fault zone permeability values (9×10^{-15} m² < k < 10^{-14} m²). Below this value, the values are close to 0, and above, the values reach 90%. The configuration with topography and reservoir (blue line) reproduces proportions close to reality, 30–35%, for fault zone permeabilities greater than 9×10^{-15} m².

1.3.2.3. Flow rates. Total outflows from the Chaudes-Aigues area are the last quantified criterion to be reproduced. In the city, these are estimated at around 700 l·min^{-1}.

Configurations without topography do not achieve a flow rate of 700 l·min^{-1} at Chaudes-Aigues, whatever the value of the permeability of the fault zone (yellow and red lines, Fig. 11d). For the two configurations with topography, flow rates reach 700 l·min^{-1} for $k_f = 9 \times 10^{-15}$ m² (case of a reservoir) and for $k_f = 10^{-14}$ m² (in the absence of a reservoir). When the fault zone permeability is very high (5×10^{-14} m²), a flow rate of 3500 l·min^{-1} is obtained (blue line, Fig. 11d) with reservoir, and 3000 l·min^{-1} without (green line, Fig. 11d).

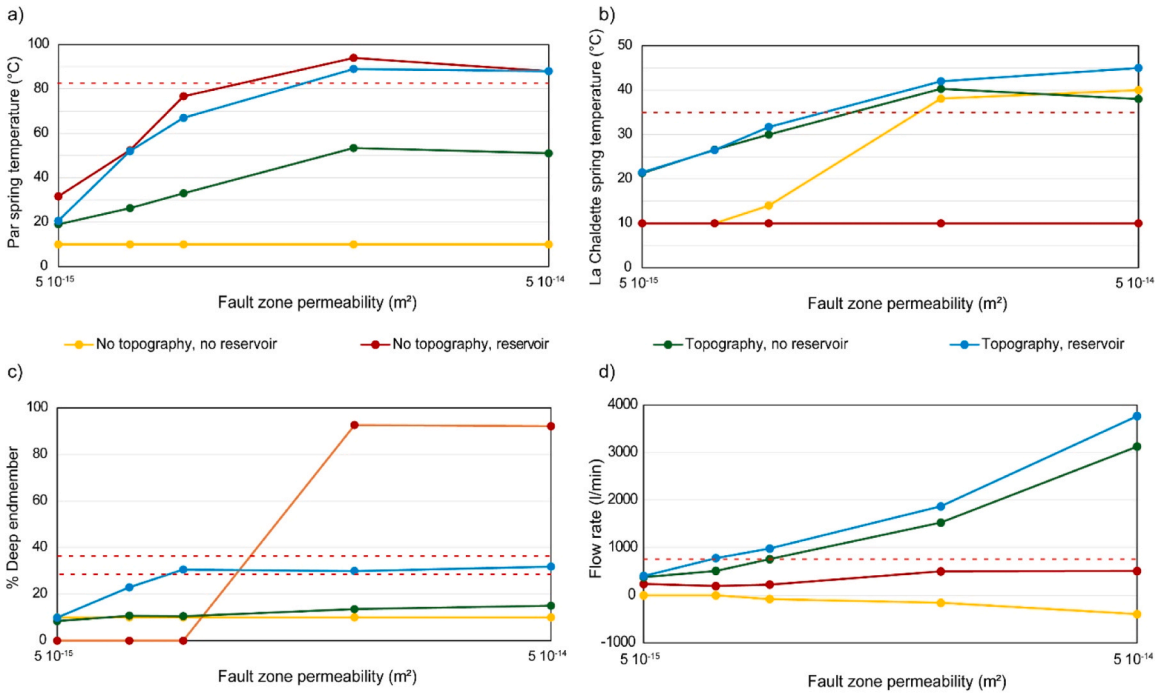

Fig. 11. Results of the different models (with/without topography, reservoir): (a) Par spring temperature, (b) La Chaldette spring temperature, (c) mixing coefficients between surface water and deep endmember, and (d) discharge rates at Chaudes-Aigues (see Fig. 7) as a function of the fault zone permeability(k_0 fault, 5×10^{-15}, 9×10^{-15}, 10^{-14}, 2×10^{-14} and 5×10^{-14} m²). Red dot line indicates the Par Spring or La Chaldette spring values observed and that must be reproduced.

1.3.2.4. Spring and impluvium locations. The geographical location of the Par Spring was reproduced for all configurations except the one without topography and without reservoir (Fig. 12a). In this configuration, the La Chaldette spring is reproduced, but water would come from Chaudes-Aigues (Fig. 12b), which is not consistent with previous studies (Penhoët et al., 2025b). Models without topography and with reservoir were unable to simulate the La Chaldette spring (Fig. 12c). However, the Par spring impluvium area is reproduced and located further south in FZ2 (Fig. 12d).

1.3.2.5. Synthesis. Fig. 13 summarises the results and the ability of the different configurations to reproduce the entire hydrothermal system. The first configuration, with no topography or reservoir, only reproduces La Chaldette spring temperature and location. The rest of the criteria are absent. Then, if a reservoir is added, still without topography, the criteria concerning the Par Spring (location, temperature and flow rates) are validated. Nevertheless, the La Chaldette spring is no longer reproduced.

The two configurations that include topography produced the best results. The first, which does not include a reservoir, meets all the criteria except for the Par Spring temperature (maximum of 50°C, green line in Fig. 11a) and the mixing coefficients (90% surface contribution, green line in Fig. 11c) for the Par. Despite these failures, the hydrothermal system is almost reproduced. The final configuration, which incorporates both a reservoir and topography, is the only one that successfully reproduces all criteria observed in the field and identified through geochemical studies.

1.4. Discussion

1.4.1. At the scale of metropolitan France

Thermal springs in France are mainly located in regions of moderate to high topography: the Massif Central, the Vosges, the Pyrenees and the Alps (Fig. 3). The aim here is to determine whether the distribution of these springs is purely random, or whether it is influenced by several specific geological factors, as suggested by Tamburello et al. (2022). Based on this study and on the updated database, this section aims to analyse the distribution of thermal springs in metropolitan France using lithology, topography, fault density and heat flow.

Our results (see section 4.1) demonstrate the complex relations between thermal springs, heat flow, lithologies, elevation changes and fault density. None of these parameters, by itself, can control the presence of a thermal spring or its temperature. Instead, a combination of several criteria appears to be favourable.

For example, mountainous regions mainly made up of basement rocks, with a high topographic gradient and high fault density, host a lot of thermal springs. In these contexts, fluid circulation is mainly driven by topography, meteoric waters infiltrate at high elevations and flowing downward along permeable structure before being discharged at lower altitudes (Taillefer et al., 2018; Carbajal-Martínez et al., 2024; Bandara et al., 2025; Serianz et al., 2025).

Conversely, basin areas (Aquitaine or Paris Basin), characterized by low relief, limited faulting and thick sedimentary cover, display few thermal springs. In these settings, buoyancy-driven flow related to deep thermal anomalies may exist, but the lack of efficient

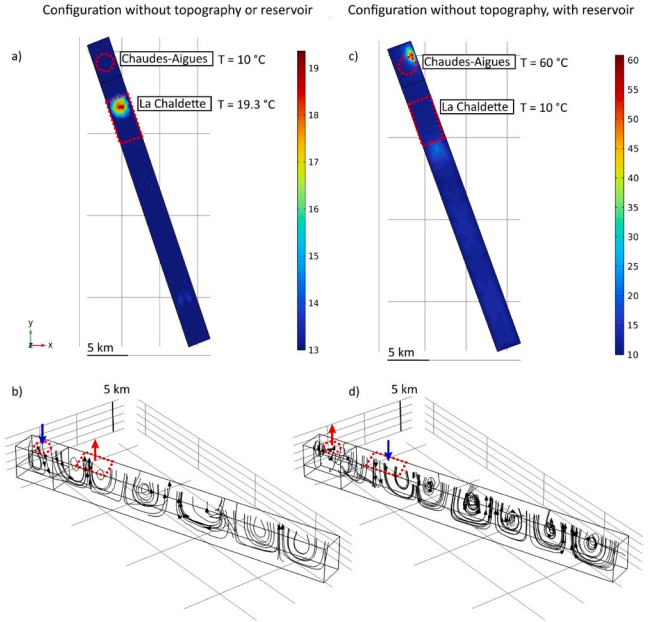

Fig. 12. Examples of configurations in which the springs and impluvium locations are not reproduced, $k_f = 9 \times 10^{-15}$ m². The red dotted lines indicate the emergence areas of Chaudes-Aigues and La Chaldette. (a) (c) Top view of the FZ2 fault zone with the computed temperatures of the springs. (b) (d) Black lines represent streamlines within FZ2. Red arrow indicates an upwelling of fluids, the blue arrow an infiltration.

Configurations				Par spring temperature	LC spring temperature	Par spring location	LC spring location	Impluvium location	Mixture proportion	Chaudes-Aigues flow rate	Conclusion
✗	Topography	✗	Reservoir								Not reproduced
✗	Topography	✓	Reservoir								Partially reproduced
✓	Topography	✗	Reservoir								Almost reproduced
✓	Topography	✓	Reservoir								Reproduced

Fig. 13. Results of the different modelling configurations in relation to the constraint parameters used. The conclusion column corresponds to the ability to reproduce the hydrothermal system at Chaudes-Aigues. LC: La Chaldette; X: not included ✓: included. Pink boxes indicated that the criterion is not reproduced (green boxes: reproduced).

vertical permeability limits the upward flow of hot fluids to reach the surface. These two examples are valid whatever the heat flow measured (e.g. low flux value in the Pyrenees but high in the south of the Paris Basin).

However, the Alps and Corsica represent an initial counterexample to this system: even with high altitudes, basement rocks and strong faulting, the number of thermal springs remains limited.

This apparent paradox can be directly related to the concept of permeability. Fault density can be used as a first-order indicator of the effective permeability of a given area, as fluid circulation in basement rocks is mainly controlled by fault networks. Thermo-hydraulic modelling has shown that there is a window of optimal permeability values (of the host rock) that allows the highest spring temperature values to be reached (Lopez and Smith, 1995). In our case, using the fracture density calculated around the emergence zone, a similar behaviour appears. If the fault density is too low, the permeability is assumed to be low, and the hot fluids rise slowly, in small volumes, and cool. As a result, surface springs will be cold. Inversely, when the fracturing density is very high, the area becomes favourable for the infiltration of dense, cold fluids because it is highly permeable. By contrast, with an intermediate fracturing density, the area becomes permeable enough to allow the fast ascent of hot fluids in large volumes, but not permeable enough to allow the infiltration of cold fluids. In this configuration, thermal springs appear.

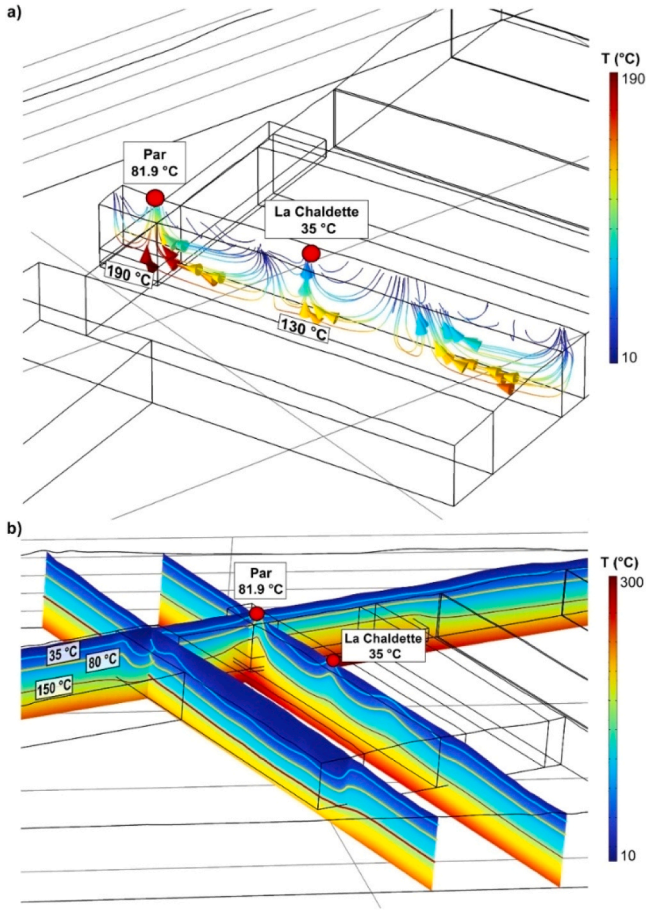

Fig. 14. Final model representing the Chaudes-Aigues hydrothermal system with $k_{FZ2} = 10^{-14}$ m², $k_{FZ1} = 5 \times 10^{-14}$ m² and h = 0.01 W.m^{-2}.K^{-1}. (a) The arrows represent streamlines (maximum value for Darcy velocity: $10^{-8.5}$ m·s^{-1}). The colour code on streamlines represents circulation temperatures in the fault zone. (b) Thermal state of the different fault zones in the model, with associated deformed isotherms.

This intermediate fracture density corresponds to a maximum permeability value of 10^{-14} m² in the Chaudes-Aigues fault zone (FZ2). For a higher permeability value (5×10^{-14} m²), downwellings are promoted, as within the FZ1 fault zone (Fig. 14). It must be noted that maximum permeability values around 10^{-14} m² have already been found to reproduce temperature profiles in geothermal systems of western Anatolia (Roche et al., 2018), as well as temperatures and locations of the thermal springs along the Têt fault, eastern Pyrenees (Taillefer et al., 2018). Magri et al. (2016) also used such values to explain locations and temperatures of clusters of springs in the Lower Yarmouk Gorge (at the border of Israel, Jordan and Syria).

1.4.2. *Chaudes-Aigues hydrothermal system*

To reproduce the exact temperatures of the Chaudes-Aigues and La Chaldette springs and flow rates at Chaudes-Aigues, models with both topography and reservoir were necessary (Fig. 14a). The result is 81.9°C at the Par Spring for a total flow rate of 800 l·min^{-1}. The proportions of the mixture remain close to those estimated by water geochemistry, with 30% of the water coming from the fault zone and 70% from the deep reservoir. In addition, the infiltration zone has been defined. Indeed, Vasseur et al. (1997) assumed a possible deep connection with the Aubrac plateau. Numerical models have shown that this is not the case, as no circulation is visible even at very low velocities. Because of its great thickness, 5 km in the models, the Aubrac becomes more favourable to downward flow, which results in a downward deformation of the isotherms (Fig. 14b). Nevertheless, the infiltration zone appears to be located north from La Chaldette spring (Fig. 14a). The N150E fault zone (FZ 2 in the model) therefore includes the infiltration, circulation and emergence zones. However, deeper and slower circulations could also originate from the southern edge of the MGC.

Vasseur et al. (1997) proposed that that present-day thermal waters originate from the end of the Würm Ice Age (around 10 000 years ago). However, the residence time for the entire circuit was estimated (using numerical modelling) between 50 000 and 200 000-years using maximum and minimum fluid velocity values (10^{-8} to 10^{-11} m·s^{-1}) and the length of circulation paths. This interval is consistent with other basement hydrothermal systems (Iwatsuki et al., 2000; Dupuy et al., 2021, Waber et al., 2017; Carbajal-Martínez et al., 2024; Wang et al., 2024) but indicates an infiltration prior to the melting of the Würm glaciers.

La Chaldette spring also comes from circulation within this N150E fault zone, with models indicating circulation reaching 130°C (Fig. 14a) at depth. This value is close to that estimated by Penhoët et al. (2025) (110 ± 10°C).

The nature of the hypothetic deep reservoir located beneath Chaudes-Aigues and more broadly along the northern edge of the MGC remains undetermined. The associated thermal springs generally align along a N050E direction, which is largely represented by faults in the study area. Circulation could therefore occur within a vast Variscan fault zone. This reservoir would maintain a temperature of 190°C at a depth of 4.5 km, temperature which is the equilibrium temperature at a depth of 6 km, the bottom of the reservoir. Consequently, upwelling hot fluids coming from a depth of 6 km would be drained by this 1.5 km thick permeable zone. The presence of a cap rock (metamorphic units) would facilitate the storage of hot fluids (190°C) at a depth of 4.5 km.

1.4.3. *Limitations and modelling perspectives*

At the scale of the hydrothermal system, the aim of this study was to assess the main factors controlling the Chaudes-Aigues hydrothermal system, through modelling using thermo-hydraulic coupling. Only the configuration incorporating both topography and a deep reservoir can reproduce all the criteria observed in the field. This configuration therefore appears to be the most realistic for representing the current hydrothermal system.

Nevertheless, several limitations need to be highlighted. The first concerns the main unknown parameter in modelling: permeability. This fundamental parameter is not constrained by laboratory measurements in our study area, and the values used are based on assumptions and correspond to those in the literature (Brace, 1984; Evans et al., 1997; Sonney and Vuataz, 2009; Ranjram et al., 2012; Walter, 2017; Achtziger-Zupančič et al., 2016; 2017; Neuzil, 2019; Duwiquet et al., 2019; Carbajal-Martínez et al., 2026). Furthermore, permeability is assumed to be laterally homogeneous in fault zones, without taking into account the alternation between fault cores (impermeable) and damage zones (permeable). Here, the value used is an average of these components.

The second limitation is the simplified geometrical representation of the fault network. The Chaudes-Aigues intersection zone is modelled as a single permeable domain. This representation may overestimate the thickness of the permeable domain which would favour hydrothermal convection (Malkovsky and Magri, 2016; Duwiquet et al., 2024; Penhoët et al., 2025a). Furthermore, the actual orientations of the two fault zones are not taken into account. However, the orientation of a fault in relation to regional tectonic constraints is a key factor influencing fluid circulation (Barton et al., 1995; McKenna and Blackwell, 2004; Faulds et al., 2010; Haines et al., 2016, Duwiquet et al., 2022). These two limitations will have to be unlocked by further thermo-hydraulic-mechanical approach to obtain more accurate results on the nature of the upwelling drains at Chaudes-Aigues.

Finally, another important limitation is that the regolith is not taken into account in the model. This weathered surface layer, often characterised by very high permeability (up to 10^{-12} m², Lachassagne et al., 2011), can play a key role in the interactions between deep and surface circulations, and can also have thermal impacts. Its exclusion from the model is a necessary compromise to avoid numerical instabilities and excessive complexity, but it limits the representation of interactions between deep flows and the infiltration zone.

1.4.4. *Implication for geothermal exploration*

Geothermal exploration is generally focused towards areas of high surface heat flow related to rifting, or magmatism associated with subduction, or hot spots triggered by mantle upwellings (Moeck, 2014; Jolie et al., 2021). Present-day spatial distribution of geothermal power plants (https://www.thinkgeoenergy.com/map/) clearly underlines such geological contexts. In the recent years, geothermal exploration enlarged the set of interesting geological settings by including anomalously permeable zones, such as crustal fault zones (Faulds et al., 2010; Bellanger et al.,2016; Duwiquet et al., 2024; Bischoff et al., 2024; Carbajal-Martínez et al., 2024; Penhoët et al., 2025a). Our study supports this observation by showing that thermal springs, surface indicators of high temperatures

thermal anomalies at depth, can develop without exceptional heat flow or elevation change but can instead result from deep fluid circulation along permeable fault zones. Chaudes-Aigues hydrothermal system represents one of these new targets of this emerging concept. Targeting anomalously permeable zones allows to explore new geological settings, including amagmatic systems in crystalline basement. In addition, thanks to the presence of highly permeable rocks, hydraulic fracturing is not necessarily required, and the occurrence of unwanted earthquakes is thus avoided.

1.5. Conclusions

This study tries to answer the fundamental question of why thermal springs emerge in certain places. Through a combination of a large-scale statistical analysis and numerical modelling, we demonstrate that the occurrence of thermal springs cannot be explained by a single controlling parameter. Our statistical analysis, based on more than 360 thermal springs across metropolitan France, reveals no dominant geological, structural or thermal control, highlighting the complex nature of hydrothermal systems.

The apparent absence of a simple factor controlling spring location is illustrated by the Chaudes-Aigues hydrothermal system, which is used here as a natural example of a fault-controlled geothermal system in an amagmatic setting. Models show that high-temperature springs can form in areas of high regional heat flow and low topography but with an important fault zone with efficient permeability.

Beyond the specific case of Chaudes-Aigues, this work establishes a robust conceptual basis for understanding and exploring geothermal systems in crystalline basement rock. It suggests that future geothermal exploration strategy should shift its focus from areas of heat flow anomalies to areas of long-lived, crustal fault zones associated with natural permeability. From this perspective, amagmatic basement hydrothermal systems emerge as a promising geothermal target that could deliver high temperature fluids without hydraulic stimulation and with reduced induced seismicity risk.

Funding

The financial support was provided by Bureau de Recherches Géologiques et Minières (BRGM), Institut des Sciences de la Terre d'Orléans (ISTO) and by the National Research Agency project « GERESFAULT » (ANR-19-CE05–0043).

CRediT authorship contribution statement

Laurent Arbaret: Writing – original draft, Supervision, Methodology, Conceptualization. **Yannick Branquet:** Writing – original draft, Methodology, Conceptualization. **Angélie Portal:** Writing – original draft, Validation. **Bernard Sanjuan:** Writing – original draft, Validation. **GUILLOU-FROTTIER Laurent:** Writing – original draft, Supervision, Software, Project administration, Methodology, Funding acquisition, Conceptualization. **Emmy Penhoët:** Writing – original draft, Software, Methodology, Investigation, Formal analysis, Data curation, Conceptualization.

Declaration of Competing Interest

The authors declare the following financial interests/personal relationships which may be considered as potential competing interests: Laurent GUILLOU-FROTTIER reports financial support was provided by Bureau for Geological and Mining Research. Laurent GUILLOU-FROTTIER reports financial support was provided by French National Research Agency. If there are other authors, they declare that they have no known competing financial interests or personal relationships that could have appeared to influence the work reported in this paper.

Acknowledgements

The authors would like to thank Andrea Moscariello, Béatrice Ledésert, Alain Dupuy, Patrick Lachassagne and Caroline Martel for the insightful and constructive discussions during the PhD defense of the first author. In addition, the authors warmly thank Audrey Taillefer, Christoph Wanner and Daniel Carbajal-Martínez for constructive comments on the first version of the manuscript.

Data availability

Data will be made available on request.

References

Achtziger-Zupančič, P., Loew, S., Hiller, A., Mariethoz, G., 2016. 3D fluid flow in fault zones of crystalline basement rocks (Poehla-Tellerhaeuser Ore Field, Ore Mountains, Germany). Geofluids 16, 688–710. https://doi.org/10.1111/gfl.12192.

Achtziger-Zupančič, P., Loew, S., Mariéthoz, G., 2017. A new global database to improve predictions of permeability distribution in crystalline rocks at site scale. J. Geophys. Res. Solid Earth 122, 3513–3539. https://doi.org/10.1002/2017JB014106.

Allen, D.M., Grasby, S.E., Voormeij, D.A., 2006. Determining the circulation depth of thermal springs in the southern Rocky Mountain Trench, south-eastern British Columbia, Canada using geothermometry and borehole temperature logs. Hydrogeol. J. 14, 159–172. https://doi.org/10.1007/s10040-004-0428-z.

Andrews, J.N., Burgess, W.G., Edmunds, W.M., Kay, R.L.F., Lee, D.J., 1982. The thermal springs of Bath. Nature 298, 339–343. https://doi.org/10.1038/298339a0.

Annales des mines, 1998. Inventaire des sources d'eau minérale naturelle en France -Réalités Industrielles. ⟨https://www.annales.org/ri/1998/ri05-98/inventaire.pdf⟩.
Bandara, D., Smit, J., Wohnlich, S., Heinze, T., 2025. Exploring a long distance, amagmatic, across-suture orogenic geothermal system: Sri Lanka's foreland hot springs. iScience 28. https://doi.org/10.1016/j.isci.2025.112370.
Barton, C.A., Zoback, M.D., Moos, D., 1995. Fluid flow along potentially active faults in crystalline rock. Geology 23, 683–686. https://doi.org/10.1130/0091-7613(1995)023<0683:FFAPAF>2.3.CO;2.
Bellanger, M., Auxiètre, J.L., Ars, J.M., Hautot, S., Tarits, P., 2016. The key role of first-order geological paradigm in deep geothermal exploration. European Geothermal Congress 2016, Strasbourg, France, 19–24 September 2016.
Bérard, P., Loiseau, M., Vigouroux, P., 2002. Amélioration de la connaissance des ressources en eau souterraine des sites thermaux – Région Auvergne – Site de Chaudes-Aigues (15). (Rapport BRGM No. RP-51722-FR). BRGM.
Bischoff, A., Heap, M.J., Mikkola, P., Kuva, J., Reuschlé, T., Jolis, E.M., Engström, J., Reijonen, H., Leskelä, T., 2024. Hydrothermally altered shear zones: a new reservoir play for the expansion of deep geothermal exploration in crystalline settings. Geothermics 118, 102895. https://doi.org/10.1016/j.geothermics.2023.102895.
Blanquet, L., Aubignat, A., Cuvelier, A., Tronche, A., De la Tour, J., 1950. Le bassin hydrothermal de Chaudes-Aigues (Cantal). Ann. Inst. Hydro 2ème Fasc. 109 à 136.
Brace, W.F., 1984. Permeability of crystalline rocks: new in situ measurements. J. Geophys. Res. 89, 4327–4330. https://doi.org/10.1029/JB089iB06p04327.
Cailleaux, P., Fouillac, C., Michard, G., Ouzounian, G., 1976. Etude géochimique des sources thermales de Chaudes-Aigues (Cantal). Conséquences géothermiques. C. R. Acad. Sci. 282, 1237–1240.
Carbajal-Martínez, D., Wanner, C., Diamond, L.W., Peiffer, L., Fletcher, J., Inguaggiato, C., Contreras-López, M., 2024. Behavior of amagmatic orogenic geothermal systems: insights from the agua blanca fault, Baja California, Mexico. Geochem. Geophys. Geosystems 25, e2023GC011145. https://doi.org/10.1029/2023GC011145.
Carbajal-Martínez, D., Wanner, C., Peiffer, L., Diamond, L.W., 2026. Behavior of coastal amagmatic geothermal systems: thermal–hydraulic modeling insights from La Jolla Beach, Baja California, Mexico. J. Geophys. Res. Solid Earth 131. https://doi.org/10.1029/2025JB033188.
Cloetingh, S., van Wees, J.D., Ziegler, P.A., Lenkey, L., Beekman, F., Tesauro, M., Förster, A., Norden, B., Kaban, M., Hardebol, N., Bonté, D., Genter, A., Guillou-Frottier, L., Ter Voorde, M., Sokoutis, D., Willingshofer, E., Cornu, T., Worum, G., 2010. Lithosphere tectonics and thermo-mechanical properties: an integrated modelling approach for Enhanced Geothermal Systems exploration in Europe. Earth-Sci. Rev. 102, 159–206. https://doi.org/10.1016/j.earscirev.2010.05.003.
De Goer de Herve, A., 1991. Carte géologique de la France à 1/50 000. feuille 813 Chaudes-Aigues.
Dèzes, P., Schmid, S.M., Ziegler, P.A., 2004. Evolution of the European cenozoic rift system: interaction of the Alpine and Pyrenean orogens with their foreland lithosphere. Tectonophysics 389, 1–33. https://doi.org/10.1016/j.tecto.2004.06.011.
Dèzes, P., Schmid, S.M., Ziegler, P.A., 2005. Reply to comments by L. Michon and O. Merle on "Evolution of the European Cenozoic Rift System: interaction of the Alpine and Pyrenean orogens with their foreland lithosphere". Tectonophysics 257–262. https://doi.org/10.1016/j.tecto.2005.01.006.
Dupuy, M., 2021. Caractérisation hydrogéologique, hydrogéochimique et isotopique des eaux souterraines thermo-minérales de la Corse orientale. Université Pascal Paoli.
Duwiquet, H., Arbaret, L., Guillou-Frottier, L., Heap, M.J., Bellanger, M., 2019. On the geothermal potential of crustal fault zones: a case study from the Pontgibaud area (French Massif Central, France). Geotherm. Energy 7, 33. https://doi.org/10.1186/s40517-019-0150-7.
Duwiquet, H., Guillou-Frottier, L., Arbaret, L., Bellanger, M., Guillon, T., Heap, M.J., 2021. Crustal fault zones (CFZ) as geothermal power systems: a preliminary 3D THM model constrained by a multidisciplinary approach. Geofluids 2021, 1–24. https://doi.org/10.1155/2021/8855632.
Duwiquet, H., Magri, F., Lopez, S., Guillon, T., Arbaret, L., Bellanger, M., Guillou-Frottier, L., 2022. Tectonic regime as a control factor for crustal fault zone (CFZ) geothermal reservoir in an amagmatic system: a 3D dynamic numerical modeling approach. Nat. Resour. Res 31, 3155–3172. https://doi.org/10.1007/s11053-022-10116-w.
Duwiquet, H., Genter, A., Guillou-Frottier, L., Donzé, F.V., Ledru, P., Magri, F., Guillon, T., Horne, R.N., Arbaret, L., Souque, C., 2024. Advanced 3D TH and THM modeling to shed light on thermal convection in fault zones with varying thicknesses. J. Geophys. Res. Solid Earth 129. https://doi.org/10.1029/2023JB028205.
Evans, J., Forster, C., Goddard, J., 1997. Permeability of fault-related rocks, and implications for hydraulic structure of fault zones. Journal of Structural Geology 19, 1393–1404. https://doi.org/10.1016/S0191-8141(97)00057-6.
Faulds, J., Coolbaugh, M., Bouchot, V., Moek, I., Oguz, K., 2010. Characterizing structural controls of geothermal reservoirs in the great basin. Developing Successful Exploration Strategies in Extended Terranes, USA, and Western Turkey.
Ferguson, G., Grasby, S.E., 2011. Thermal springs and heat flow in North America. Geofluids 11, 294–301. https://doi.org/10.1111/j.1468-8123.2011.00339.x.
Foued, B., Hénia, D., Lazhar, B., Nabil, M., Nabil, C., 2017. Hydrogeochemistry and geothermometry of thermal springs from the Guelma region, Algeria. Jour. Geol. Soc. India 90, 226–232. https://doi.org/10.1007/s12594-017-0703-y.
Gibert, J.P., Sorel, D., Vergely, P., 1975. Tectonique cassante polyphasée et émergences d'eaux hyperthermales; le site de Chaudes-Aigues (Cantal). Bull. De. la Soci. été Géologique De. Fr. S7-XVII, 629–636. https://doi.org/10.2113/gssgfbull.S7-XVII.4.629.
Grasby, S.E., Hutcheon, I., 2001. Controls on the distribution of thermal springs in the southern Canadian Cordillera. Can. J. Earth Sci. 38, 427–440. https://doi.org/10.1139/e00-091.
Guillou-Frottier, L., Carrè, C., Bourgine, B., Bouchot, V., Genter, A., 2013. Structure of hydrothermal convection in the Upper Rhine Graben as inferred from corrected temperature data and basin-scale numerical models. J. Volcanol. Geotherm. Res. 256, 29–49. https://doi.org/10.1016/j.jvolgeores.2013.02.008.
Guillou-Frottier, L., Duwiquet, H., Launay, G., Taillefer, A., Roche, V., Link, G., 2020. On the morphology and amplitude of 2D and 3D thermal anomalies induced by buoyancy-driven flow within and around fault zones. Solid Earth 11, 1571–1595. https://doi.org/10.5194/se-11-1571-2020.
Guillou-Frottier, L., Milesi, G., Roche, V., Duwiquet, H., Taillefer, A., 2024. Heat flow, thermal anomalies, tectonic regimes and high-temperature geothermal systems in fault zones. C. R. Geosc 356, 1–33. https://doi.org/10.5802/crgeos.213.
Haines, S., Lynch, E., Mulch, A., Valley, J.W., Van Der Pluijm, B., 2016. Meteoric fluid infiltration in crustal-scale normal fault systems as indicated by δ^{18}O and δ^{2}H geochemistry and ^{40}Ar/^{39}Ar dating of neoformed clays in brittle fault rocks. Lithosphere 8, 587–600. https://doi.org/10.1130/L483.1.
Ingebritsen, S.E., Manning, C.E., 2010. Permeability of the continental crust: dynamic variations inferred from seismicity and metamorphism. Geofluids 10, 193–205. https://doi.org/10.1111/j.1468-8123.2010.00278.x.
Iwatsuki, T., Xu, S., Itoh, S., Abe, M., Watanabe, M., 2000. Estimation of relative groundwater age in the granite at the Tono research site, central Japan. Nucl. Instrum. Methods Phys. Res. Sect. B Beam Interact. Mater. At. 8th Int. Conf. Accel. Mass Spectrom. 172, 524–529. https://doi.org/10.1016/S0168-583X(00)00149-X.
Jenks, G.F., 1967. The data model concept in statistical mapping. Int Yearb. Cartogr. 7, 186–190.
Jolie, E., Scott, S., Faulds, J., Chambefort, I., Axelsson, G., Gutiérrez-Negrín, L., Regenspurg, S., Ziegler, M., Ayling, B., Richter, A., Zemedkun, M., 2021. Geological controls on geothermal resources for power generation. Nat. Rev. Earth Environ. 2, 324–339. https://doi.org/10.1038/s43017-021-00154-y.
Jolivet, L., Faccenna, C., Becker, T., Davaille, A., Lasseur, E., Briais, J., Koptev, A., Sternai, P., Le Pourhiet, L., 2025. Continental rifts and mantle convection. Earth-Sci. Rev. 270, 105243. https://doi.org/10.1016/j.earscirev.2025.105243.
Lachassagne, P., Wyns, R., Dewandel, B., 2011. The fracture permeability of Hard Rock Aquifers is due neither to tectonics, nor to unloading, but to weathering processes. Terra Nova 23, 145–161. https://doi.org/10.1111/j.1365-3121.2011.00998.x.
Launay, G., 2018. Hydrodynamique des systèmes minéralisés péri-granitiques: étude du gisement à W-Sn-(Cu) de Panasqueira. Université d'Orléans, Portugal.
López, D., Smith, L., 1995. Fluid flow in fault zones: analysis of the interplay of convective circulation and topographically driven groundwater flow. Water Resour. Res. 31, 1489–1503. https://doi.org/10.1029/95WR00422.
Lucazeau, F., Vasseur, G., 1989. Heat flow density data from France and surrounding margins. Tectonophysics 164, 251–258. https://doi.org/10.1016/0040-1951(89)90018-8.
Lucazeau, F., Vasseur, G., Bayer, R., 1984. Interpretation of heat flow data in the French Massif Central. Tectonophys. Terr. Heat. Flow. Stud. Struct. Lithos 103, 99–119. https://doi.org/10.1016/0040-1951(84)90077-5.

Magri, F., Möller, S., Inbar, N., Möller, P., Raggad, M., Rödiger, T., Rosenthal, E., Siebert, C., 2016. 2D and 3D coexisting modes of thermal convection in fractured hydrothermal systems - implications for transboundary flow in the Lower Yarmouk Gorge. Mar. Pet. Geol. 78, 750–758. https://doi.org/10.1016/j.marpetgeo.2016.10.002.

Majorowicz, J., Wybraniec, S., 2011. New terrestrial heat flow map of Europe after regional paleoclimatic correction application. Int J. Earth Sci. (Geol. Rundsch.) 100, 881–887. https://doi.org/10.1007/s00531-010-0526-1.

Malkovsky, V., Magri, F., 2016. Thermal convection of temperature-dependent viscous fluids within three-dimensional faulted geothermal systems: estimation from linear and numerical analyses. Water Resour. Res. 52, 2855–2867. https://doi.org/10.1002/2015WR018001.

McKenna, J., Blackwell, D., 2004. Numerical modeling of transient Basin and Range extensional geothermal systems. Geothermics 33, 457–476. https://doi.org/10.1016/j.geothermics.2003.10.001.

Merle, O., Aumar, C., Labazuy, P., Merciecca, C., Buvat, S., 2023. Structuration tertiaire et quaternaire du Plateau des Dômes (Chaîne des Puys, Massif central, France). Géologie De. la Fr.

Michon, L., Merle, P., 2005. Discussion on “evolution of the European Cenozoic Rift System: interaction of the Alpine and Pyrenean orogens with their foreland lithosphere” by P. Dèzes, S.M. Schmid and P.A. Ziegler, Tectonophysics 389 (2004) 1–33. Tectonophysics 401, 251–256. https://doi.org/10.1016/j.tecto.2005.01.006.

Michon, L., Van Balen, R.T., Merle, O., Pagnier, H., 2003. The cenozoic evolution of the roer valley rift system integrated at a European scale. Tectonophysics 367, 101–126. https://doi.org/10.1016/S0040-1951(03)00132-X.

Moeck, I.S., 2014. Catalog of geothermal play types based on geologic controls. Renew. Sustain. Energy Rev. 37, 867–882. https://doi.org/10.1016/j.rser.2014.05.032.

Neuzil, C.E., 2019. Permeability of clays and shales. Annu. Rev. Earth Planet. Sci. 47, 247–273. https://doi.org/10.1146/annurev-earth-053018-060437.

Penhoët, E., Arbaret, L., Guillou-Frottier, L., Duwiquet, H., Gumiaux, C., Bellanger, M., 2025a. Fluid flow in crustal fault zones with varying lengthwise thickness: application to the Margeride fault zone (French Massif Central). Geotherm. Energy 13, 6. https://doi.org/10.1186/s40517-025-00334-9.

Penhoët, E., Arbaret, L., Portal, A., Gumiaux, C., Canva, A., Picault, M., Maubec, N., Caritg, S., Guillou-Frottier, L., 2026. Long-lived brittle reactivation of crossing fault networks enhancing upwellings in hydrothermal systems: The case study of Chaudes-Aigues spring swarm. Geothermics 139, 103679. https://doi.org/10.1016/j.geothermics.2026.103679.

Penhoët, E., Sanjuan, B., Guillou-Frottier, L., Arbaret, L., Moreira, M., 2025b. One hydrothermal system may hide another: Insights from a geochemical exploration of Chaudes-Aigues and nearby springs (French Massif Central). Geothermics 133, 103476. https://doi.org/10.1016/j.geothermics.2025.103476.

Rabinowicz, M., Boulègue, J., Genthon, P., 1998. Two- and three-dimensional modeling of hydrothermal convection in the sedimented Middle Valley segment, Juan de Fuca Ridge. J. Geophys. Res. 103, 24045–24065. https://doi.org/10.1029/98JB0148.

Ranjram, M., Gleeson, T., Luijendijk, E., 2012. Is the permeability of crystalline rock in the shallow crust related to depth, lithology, or tectonic setting? in: Crustal Permeability. John Wiley & Sons, Ltd, pp. 123–136. https://doi.org/10.1002/9781119166573.ch12.

Roche, V., Sternai, P., Guillou-Frottier, L., Menant, A., Jolivet, L., Bouchot, V., Gerya, T., 2018. Emplacement of metamorphic core complexes and associated geothermal systems controlled by slab dynamics. Earth Planet. Sci. Lett. 498, 322–333. https://doi.org/10.1016/j.epsl.2018.06.043.

Saar, M.O., Manga, M., 2004. Depth dependence of permeability in the Oregon Cascades inferred from hydrogeologic, thermal, seismic, and magmatic modeling constraints. J. Geophys. Res. Solid Earth 109. https://doi.org/10.1029/2003JB002855.

Serianz, L., Markelj, A., Rman, N., Brenčič, M., Mádl-Szőnyi, J., 2025. Hydrogeological analysis of topography-driven groundwater flow in a low temperature geothermal aquifer system in the Julian Alps, Slovenia. Hydrogeol. J. 33, 237–256. https://doi.org/10.1007/s10040-024-02866-z.

Sonney, R., Vuataz, F.-D., 2009. Numerical modelling of Alpine deep flow systems: a management and prediction tool for an exploited geothermal reservoir (Lavey-les-Bains, Switzerland). Hydrogeol. J. 17, 601–616. https://doi.org/10.1007/s10040-008-0394-y.

Stober, I., Zhong, J., Zhang, L., Bucher, K., 2016. Deep hydrothermal fluid–rock interaction: the thermal springs of Da Qaidam, China. Geofluids 16, 711–728. https://doi.org/10.1111/gfl.12190.

Taillefer, A., Guillou-Frottier, L., Soliva, R., Magri, F., Lopez, S., Courrioux, G., Millot, R., Ladouche, B., Le Goff, E., 2018. Topographic and faults control of hydrothermal circulation along dormant faults in an Orogen. Geochem Geophys Geosyst 19, 4972–4995. https://doi.org/10.1029/2018GC007965.

Taillefer, A., Truche, L., Audin, L., Donzé, F.-V., Tisserand, D., Denti, S., Manrique Llerena, N., Masías Alvarez, P., Braucher, R., Zerathe, S., Monnin, C., Dutoit, H., Taipe Maquerhua, E., Apaza Choquehuayta, F., 2024. Characterization of Southern Peru hydrothermal systems: new perspectives for geothermal exploration along the andean forearc. e2023GC011344 Geochem. Geophys. Geosystems 25. https://doi.org/10.1029/2023GC011344.

Talbot, J.Y., Faure, M., Chen, Y., Martelet, G., 2005. Pull-apart emplacement of the Margeride granitic complex (French Massif Central). Implications for the late evolution of the Variscan orogen. J. Struct. Geol. 27, 1610–1629. https://doi.org/10.1016/j.jsg.2005.05.008.

Tamburello, G., Chiodini, G., Ciotoli, G., Procesi, M., Rouwet, D., Sandri, L., Carbonara, N., Masciantonio, C., 2022. Global thermal spring distribution and relationship to endogenous and exogenous factors. Nat. Commun. 13, 6378. https://doi.org/10.1038/s41467-022-34115-w.

Vasseur, G., Michard, G., Fouillac, C., 1997. Contraintes sur la structure profonde et le fonctionnement du système hydrothermal de Chaudes-Aigues (France). Hydrog. éologie 3, 17.

Waber, H.N., Schneeberger, R., Mäder, U.K., Wanner, C., 2017. Constraints on evolution and residence time of geothermal water in granitic rocks at grimsel (Switzerland). In: Procedia Earth and Planetary Science, WRI-15 17. 15th Water-Rock Interaction International Symposium, pp. 774–777. https://doi.org/10.1016/j.proeps.2017.01.026.

Walter, B., 2017. Réservoirs de socle en contexte extensif: genèse, géométries et circulations de fluides: exemples du rift intracontinental. du lac Albert (Ouganda) et de la marge proximale d’Ifni. Université de Lorraine, Maroc.

Wang, L., Liu, K., Ma, Y., Zhang, Y., Tong, J., Jia, W., Zhang, S., Sun, J., 2024. Geochemical and isotopic techniques constraints on the Origin, evolution, and residence time of low-enthalpy geothermal water in Western Wugongshan, SE China. Acta Geol. Sin. - Engl. Ed. 98, 801–818. https://doi.org/10.1111/1755-6724.15161.

Waring, G.A., Blankenship, R.R. revised by, Bentall, R., 1965. Thermal springs of the United States and other countries of the world; a summary (No. 492), Professional Paper. U.S. Govt. Print. Off.,. ⟨https://doi.org/10.3133/pp492⟩.

Zhou, X., Zhuo, L., Wu, Y., Tao, G., Ma, J., Jiang, Z., Sui, L., Wang, Y., Wang, C., Cui, J., 2023. Origin of some hot springs as conceptual geothermal models. J. Hydrol. 624, 129927. https://doi.org/10.1016/j.jhydrol.2023.129927.

Ziegler, P.A., 1992. European Cenozoic rift system. Tectonophys. Geodyn. Rift. Vol. 1 Case Hist. Stud. Rift. Eur. Asia 208, 91–111. https://doi.org/10.1016/0040-1951(92)90338-7.

Ziegler, P.A., Dèzes, P., 2007. Cenozoic uplift of Variscan Massifs in the Alpine foreland: timing and controlling mechanisms. Glob. Planet. Change 58, 237–269. https://doi.org/10.1016/j.gloplacha.2006.12.004.

IGN, 2011. BD ALTI® | Géoservices. Institut National de l’Information Géographique et Forestière, France Géoservices IGN, BD ALTI 25m, V2.0. https://geoservices.ign.fr/bdalti.